Procuring Flexibility in Power Systems with Incentive-based Grid Access Requests

Mohsen Banaei[a], Francesco D'Ettorre[a], Razgar Ebrahimy[a], Mads R. Almassalkhi[b], Henrik Madsen[a]

[a]*Technical University of Denmark, Department of Applied Mathematics and Computer Science, Copenhagen, Denmark*
[b]*University of Vermont, College of Engineering and Mathematical Sciences, Burlington, USA*

Abstract

Demand-side flexibility is an important tool for enhancing the interaction of renewable energy resources and reducing the need for grid upgrades. To employ this flexibility as a market product, it is necessary to aggregate and coordinate by coordinating responsive loads. In this regard, designing effective load coordination mechanisms that consider the preferences of aggregators, end-users, and network operators is critical for the successful implementation of demand response (DR) programs. This paper proposes an incentive-based method for coordinating a group of controllable devices that is practical, does not require complex, high-order models of the entire system, respects end-users privacy and quality of service (QoS), and can readily incorporate network conditions to ensure grid reliability. The proposed method includes algorithms at both the end-user level for controllable device operation and the aggregator level for managing the grid access requests. These algorithms are fast and with low computational burden which makes them suitable for the designed framework, reduces the implementation cost and increases the chance of scalability. The method is illustrated with a realistic test system consisting of a set of controllable heat pumps used in pool heating systems and uncontrollable loads placed in a distribution feeder and supplied by a distribution substation transformer. Simulation results highlight the effectiveness of the proposed method in satisfying the controllable device, end-users, and grid constraints. Comparing the results with similar existing methods shows that the method is 11% more cost-effective than traditional ON/OFF methods while reducing the number of rejected grid access requests from the devices, significantly.

Keywords: Demand dispatch, Demand-side flexibility, Incentive-based coordination, Load control, Grid access requests, Heat pump.

1. Introduction

In recent years, demand response (DR) techniques have been widely recognized for enabling the active participation of demand side resources in grid balancing and operations. DR consists in adapting demand profiles to grid needs, by increasing, reducing, or shifting the amount of energy consumed [1]. Although the concept of shedding large industrial loads for supporting the operation of the power grid is not a new one, modern DR involves customers of all sectors and promotes more dynamic participation in grid operations. While supply-side resources, like traditional power plants, are relatively

few in number and characterized by high power capacities, demand-side resources show opposite features: large numbers and low capacities [2]. As a consequence, aggregation and coordination mechanisms are needed to achieve a significant load modulation and to deliver value to ancillary service markets [3]. Moreover, it is worth underlining that such mechanisms have to be capable of unlocking demand-side flexibility without compromising end-users' comfort and privacy and cost-effective in both deployment and implementation, at scale.

Over the past decades, several works have focused on the coordination of demand-side resources. Coordination mechanisms can be classified into three main groups: "centralized", "decentralized", and "distributed"[1].

In centralized coordination, a central coordinator, with complete information and full controllability over all/individual devices in a population, drive the behavior of the population by broadcasting control signals in a top-down fashion. The control signals are usually derived from the solution of a centralized optimization problem (e.g., an optimal scheduling problem) and broadcast through a communication infrastructure between the central coordinator and the individual devices. In power grids, direct load control (DLC) has been one of the early methods to implement centralized methodologies, such as interruptible load schemes encouraging end users to shed their load during critical peak hours. Such mechanisms have been in place for large industrial and commercial customers for more than 50 years [5], and have received increased attention for their potential applications in the residential sector in recent years [6]. It is worth underlining that the centralized methods' requirements of complete information and full controllability may pose challenges in terms of scalability and cyber-security [7]. Indeed, the larger the population, the higher the computational burden. Moreover, it has been shown that centralized control may cause unwanted load synchronization and oscillatory effects: e.g., the rebound effect following a load curtailment event can result in a load peak higher than the one which originated the need for the demand-response event [6].

Conversely, in decentralized models, each load is equipped with a local controller which operates according to local sensing and control objectives. This avoids the need for complex computation and communication that characterizes a centralized control architecture [8]. Decentralized methods are also more resilient to cyber-attack and communication failures [9]. However, the capability of decentralized control approaches may be limited compared with more centralized approaches. This is due to the limited system-level information that the local controllers have [7].

Distributed coordination combines elements from centralized and decentralized approaches by having a centralized agent coordinate a population of loads, where each load is equipped with local sensing and control capabilities. In general, the centralized agent uses incentives such as price to interact with loads and affect their control strategy. Arroyo et al. [10] proposed a distributed control architecture to steer flexibility of buildings and track a reference load profile. In the proposed framework, an upper-level agent receives grid flexibility requests, then, virtual price signals are used to promote the desired

---

[1]It is worth underlining that the definition of decentralized and distributed is not unified in the literature. Hereinafter, we refer to the definition adopted from the optimization community [4], where distributed mechanisms enable a small amount of central coordination activity, while decentralized mechanisms rely on neighbor-to-neighbor communication only.

load variation while leaving buildings the freedom to decide their own control approach. Gupta et al. [11] introduced a method for coordinating incentive-based demand response and batteries for providing frequency regulation service in low inertia isolated grids. A price elasticity model was used to calculate incentives that should be sent to the loads for utilizing the required demand response. An incentive-based coordination mechanism for integrated electricity and heat systems was introduced by Zheng et al [12]. In this approach, price incentives are offered to district heating companies to encourage pipeline energy storage utilization and flexibility provision from district heating networks. The problem was formulated as a bi-level model. Yu et al. [13] proposed a price-based approach for utilizing the flexibility of industrial and residential customers in the intraday market. The problem was formulated as a Stackelberg game and the existence and uniqueness of the Stackelberg Equilibrium were investigated. Zhong et al. [14] proposed a coupon incentive-based demand response approach in which consumers receive a flat rate price for electricity consumption and a coupon price for modifying their baseline. These coupons are used as incentives that encourage consumers to reduce their consumption when wholesale electricity market prices spikes. The consumers are allowed to update their response to these coupons several times until the operating interval Junker et al. [15] proposed a dynamic flexibility model termed "Flexibility Function", which predicts demand as a function of prices. The Flexibility Function could be any dynamic model. In [15], a finite impulse response model is suggested, while in [16], a grey-box model based on stochastic differential equations is used. Once the Flexibility Function is estimated, it can be used to generate the price signals that should be used to indirectly control the demand to achieve some specific control objective. In [17] a centralized controller is used to coordinate a pool of thermostatically controlled loads (TCLs) to manage frequency and energy imbalance in power systems. A Markov chain model was used to describe the dynamic of the thermostatically Controlled Load (TCL) population, and a proportional controller was used to broadcast control signals (i.e. the fraction of TCLs to be switched on/off) to the TCL population to track a reference power consumption profile. Despite the good tracking performances (power tracking error ranging between 0.26 and 9.3%), the proposed control approach requires an observable model, which is not always available [18]. A similar distributed approach based on mean-field theory to control deferrable loads to deliver ancillary grid services was proposed by Meyn et al. [18, 19] and by Mathieu et al. [17].

In contrast to the above-mentioned works, in which a central load coordinator broadcasts the control signal to the population of loads (in a top-down fashion), bottom-up demand management schemes build on methods used to manage data packets in communication networks and have been widely investigated in [20–25]. Zhang and Baillieul [20, 21] proposed a bottom-up approach in which each load stochastically requests an energy packet from the coordinator based on the load's local state variables. The proposed approach, referred to as "packetized direct load control", assumed exact knowledge of the number of packetized loads at any given time, that one could queue up requests for synchronous allocation. In parallel with [20, 21], Frolik and Hines [26] proposed a random access approach for managing the charging of Plug-in Electric Vehicles (PEVs) that simultaneously avoids overloads and provides equal access to the charging resources.

Separately, Almassalkhi et al. developed Packetized Energy Management (PEM) in [20] that improves upon the above-mentioned assumptions. Under PEM, the load makes

3

requests under a generalized *need for energy* device state that has been applied for EVs, TCLs, and batteries. The PEM coordinator then either grants or denies each stochastic grid access request based on the tracking error for a power reference signal that is representative of grid and/or market conditions. That is, PEM represents a privacy-aware, asynchronous, and stochastic, bottom-up control scheme for many different switching loads, [22] [23]. QoS constraints were also considered. In [24], the macro-model methodology of the PEM system presented in [22] is further extended to model and analyze fleets of deferrable loads, such as electric vehicles (EVs). The PEM approach has also been extended to provide grid services. In [25] a methodology is proposed to estimate and provide fast frequency response (FFR) services via decentralized control of active packet interruptions. In [27] a generalization of PEM is presented which gives grid-aware load dispatch capability to the approach by incorporating a new grid constraint management algorithm. The method is capable of providing grid voltage regulation and tracking reference (e.g., AGC signals) services while guaranteeing QoS for end-users.

A summary of the literature review is presented in Table 1. It can be seen that only incentive-based methods can preserve privacy, be responsive to external incentives, and provide look-ahead capability, i.e., the ability to consider future changes in the user comfort constraint in the method, preserve privacy, and be responsive to external incentives. However, these approaches are very complex and expensive to implement, and since they modify the price to change the consumers' electricity consumption, they might not be fair for end-users. On the other hand, PEM solutions have low computational complexity, low hardware installation cost, scalability, ensure service quality, and preserve end-users privacy, but are capable of accounting for external incentives, such as electricity prices or CO_2 emissions. Moreover a device operating under PEM (i.e., a "packetized" load) has always relied on measurements of the current energy state or *need for energy* in deciding packet request probabilities and opt-out transitions and has not incorporated any look-ahead capability at the device layer.

Table 1: Summary of literature review.

Reference No.	Control architecture	Modeling complexity	Look-ahead capability	Privacy preservation	Incentives responsiveness
[5]	Centralized	High	Yes	No	Yes
[7]	Hybrid	Medium	Yes	Partially	No
[8]	Decentralized	Medium	Yes	Partially	No
[9]	Distributed	High	Yes	Partially	No
[10]	Distributed	Medium	Yes	Partially	Yes
[11]	Distributed	High	No	No	Yes
[12-16]	Distributed	High	Yes	Yes	Yes
[17-19]	Distributed	Medium	No	No	No
[20-25]	Distributed	Low	No	Yes	No
This method	Distributed	Low	Yes	Yes	Yes

To fill the gap in the literature i.e., a method with low complexity, look-ahead capability, privacy preservation, and external incentive responsiveness, this manuscript presents a bottom-up methodology inspired by PEM for coordinating grid access requests that in-

corporates incentives-based grid access requests (IBGARs) and accounts for both system-wide grid conditions and local QoS. The specific contributions of this manuscript are:

- a novel incentive-based coordination mechanism that extends prior literature (PEM method) on grid access requests;

- a look-ahead capability for taking into account known, but time-varying future changes in local QoS requirements in determining local device actions;

- adapting the device-level PEM algorithm to swimming pool heating systems with time-varying boundary conditions supplied by heat pumps.

- incorporation of system-wide constraints, such as a transformer capacity limit, to mitigate overloading;

The remainder of this paper is structured as follows. Section 2 introduces the theoretical framework of the proposed control architecture, together with the mathematical models and algorithms used in the paper. Next, Section 3 introduces the case study and presents the simulation results. Finally, Section 4 summarizes the main findings of the work and provides future research directions.

2. Incentive-based Grid Access Requests (IBGAR) framework

The required framework for implementation of the IBGAR method is illustrated in Figure 1. The main focus of this work is on developing novel algorithms for the packetized energy controller in the device layer and the flexibility management system in the coordinator layer. The sequence of actions in the proposed method is as follows:

- At each device, the real-time data of the metering devices are sent to the Device controller,

- The device controller receives the data and incentive and decides about sending or not sending a grid access request or opting out of the program temporarily,

- The result of step 2 is sent to the flexibility management system at the coordinator level,

- The flexibility management system considers a time period and collects all the asynchronous requests,

- Taking into account the reference dispatch signal received from DSO or DSO, the flexibility management system determines the accepted and rejected requests and sends the results back to devices,

- Based on the received response, the device controller generates the control signal for the device.

Detailed descriptions of the IBGAR scheme at device and coordinator levels are presented in Sections 2.1 and 2.2, respectively.
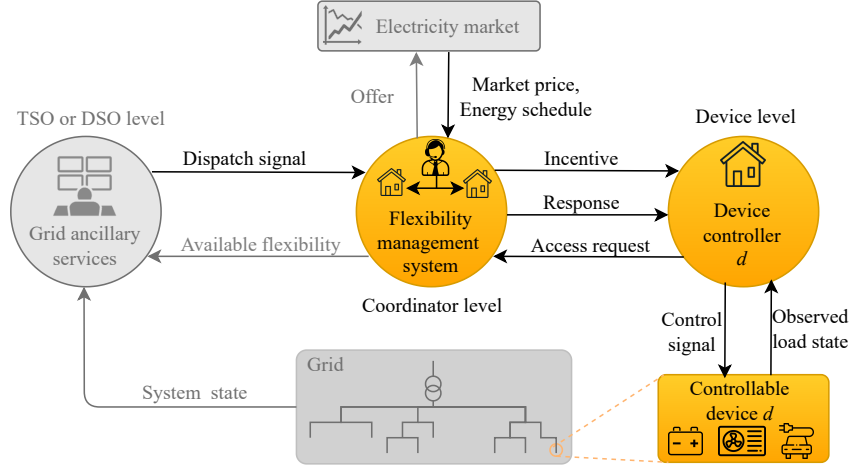
Figure 1: IBGAR framework. The orange-filled blocks represent the focus of this manuscript.

2.1. IBGAR implementation at the device level

As shown in Fig. 1, at the device level, each device controller d receives the load status information from controllable device d and the external incentive from the aggregator. Then, the device controller decides whether to send or not send a grid access request to the aggregator considering the operation cost and constraints. Finally, the received response from the aggregator is applied to the device through the control signal. To ensure the quality of service, an opt-out possibility is considered that enables the device controller to exit the energy schedule temporarily and satisfy the comfort constraints of residents or operational limitations of devices.

Figure 2 gives an overview on how the device controller decides about sending access requests. To make the decision, a stochastic request rate (SRR) function and a function that links the external incentive to an access request mechanism (ARM) are needed. The output of the ARM is a random number between 0 and 1. If this random number is less than the value of the SRR function at the measured state variable, the grid access request will be sent to the aggregator. This leads to a computationally lightweight algorithm that does not require powerful and expensive hardware for installation and a complex model of the system, can be easily applied to different devices, and is real-time responsive to external incentives.
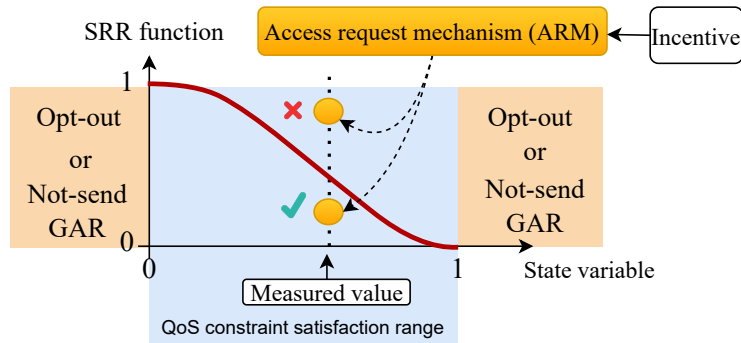

Figure 2: Overview of device controller logic showing both request and opt-out mechanisms as functions of the measured state (QoS).

If the normalized value of the state variable is negative or greater than one, the algorithm will opt out of the program or not send a grid access request (depending on the device) such that the state variable returns to the range of zero and one as soon as possible.

The definition of state variable is different for each type of controllable device. For instance, for a battery, the state variable is the state of charge (SOC), and for a TCL, the temperature represents the state variable of the load.

The method is designed in such a way that it works with normalized values of state variable and external incentives. This makes the approach generic for different applications.

The key important points for successful implementation of the method are designing the SRR function and defining the link between external incentive and the ARM which are discussed in the next subsections.

2.1.1. SRR function modeling

In IBGAR, our focus is on one specific state variable of the system x_d^* of the controllable device and the decision making is performed based on the status of this state variable. As mentioned before, the SRR function works with normalized state variable x_d^*. Using the state variable in the normalized form makes the method independent from the type of the state variable e.g., temperature, state of charge, etc., and scales it between zero and one which makes the method generic for any application.

Normalized value of the state variable x_d^* in time interval k i.e., $x_d^n[k]$ for device d is calculated as below:

$$x_d^n[k] = \frac{x_d^*[k] - x_d^{min}}{x_d^{max} - x_d^{min}}, \tag{1}$$

where x_d^{min} and x_d^{max} are the lower and upper bounds of the state variable at device d, respectively. The SRR function represents the probability of sending a grid access request at different values of the normalized state variable. Depending on the device and the control action, the SRR function should be monotonically increasing or decreasing. For a battery and charging (discharging) action, when the SOC is low the probability of sending a request is high (low) and decreases (increases) as the SOC of the battery increases, hence the SRR function with be monotonically increasing (decreasing). For a TCL and for heating (cooling) action, if the temperature is low, the probability of sending a grid access request will be high (low) and by increasing the temperature, this probability will decrease (increase), which leads to a monotonically increasing (decreasing) SRR function.

The following mathematical equation is used to formulate SRR function:

$$P(x_d^n[k]) = 1 - e^{-\mu(x_d^n[k])\Delta t}, \tag{2}$$

where $\mu(x_d^n[k])$ is the rate parameter. If the SRR function should be monotonically increasing, $\mu(x_d^n[k])$ can be formulated as below:

$$\mu(x_d^n[k]) = \begin{cases} 0 & x_d^n[k] \leq 0 \\ m_R(\frac{x_d^n[k]}{1-x_d^n[k]})(\frac{1-x_d^{set}}{x_d^{set}}) & x_d^n[k] \in (0,1) \\ \infty & x_d^n[k] \geq 1 \end{cases} . \tag{3}$$

Otherwise, $\mu(x_d^n[k])$ can be formulated as following:

$$\mu(x_d^n[k]) = \begin{cases} 0 & x_d^n[k] \geq 1 \\ m_R\left(\frac{1-x_d^n[k]}{x_d^n[k]}\right)\left(\frac{x_d^{set}}{1-x_d^{set}}\right) & x_d^n[k] \in (0,1) \\ \infty & x_d^n[k] \leq 0 \end{cases} \tag{4}$$

where x_d^{set} is the normalized desirable set point of the state variable. If a device does not have a set point for the state variable such as batteries, we should have $x_d^{set} = 0.5$. m_R is a design parameter that can be used to manage the variation of state variable around the set point and consequently manage the energy consumption of the scheme. This feature will be discussed in detail in Section 3. Three realizations of equation (2) for a decreasing SRR function are depicted in Figure 3.
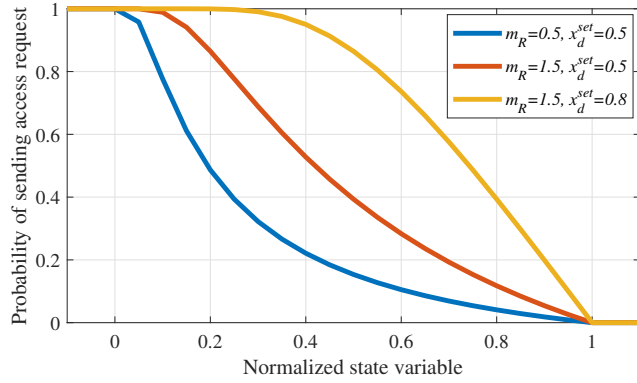
Figure 3: Illustrating the effect of m_R and x_d^{set} on the probability of sending access request for decreasing access request rates.

As shown in Figure 3, the probability of sending an access request increases by increasing the value of m_R which means more requests for energy packets and consequently more energy consumption. For the same values of m_R, the probability of sending an access request at the set point temperature is the same at different values of the set point.

2.1.2. Incorporating external incentives into the ARM

We start with normalizing the external incentives. The normalization is done such that it can deal with both dynamic and flat incentives. So, the following formulation is proposed to normalize the incentives:

$$\rho_z[k] = \frac{\rho[k]}{\frac{1}{2}(\rho^{max} + \rho^{min})} - 1, \tag{5}$$

$$\rho^n[k] = \begin{cases} \frac{\rho_z[k]}{\rho_z^{min}} & \rho_z[k] < 0 \\ \frac{\rho_z[k]}{\rho_z^{max}} & \rho_z[k] > 0 \\ 0 & \rho_z[k] = 0 \end{cases} \tag{6}$$

where $\rho[k]$ is the incentive in time interval k. ρ^{max} and ρ^{min} are the maximum and minimum values of the incentive in the time series, respectively. ρ_z^{max} and ρ_z^{min} represent the maximum and minimum of $\rho_z[k]$.

8

Using (5) and (6), for dynamic tariffs, we have $-1 \leq \rho^n[k] \leq 1$, and for fixed tariffs $\rho^n[k] = 0$.

One of the main differences between distributed coordination mechanisms (and more specifically, PEM) and the proposed IBGAR approach is incorporating external incentives in the decision making process. In PEM, the ARM works based on generating a random number $R \in [0, 1]$ using the uniform distribution [22]. In IBGAR, it is suggested that the uniform distribution is replaced with another distribution whose characteristics change as the external incentive changes. It is worth mentioning that the incentives are sent to motivate the end-users to reduce their consumption. So, assigning greater values for incentives (e.g. higher electricity prices) means more interest in reducing the energy consumption. Therefore, the characteristics of the distribution should be changed in such a way that when the incentive is high (low), there will be a higher probability for generating random numbers close to one (zero) and consequently, not sending (sending) an access request (see Figure 2). To this end, use of Beta distribution is suggested for generating the random numbers. Beta distribution is formulated as below:

$$ f(w) = \begin{cases} \frac{w^{\alpha-1}(1-w)^{\beta-1}}{B(\alpha,\beta)} & 0 \leq w \leq 1 \\ 0 & \text{otherwise} \end{cases}, \qquad \text{where } B(\alpha, \beta) = \int_0^1 v^{\alpha-1}(1-v)^{\beta-1}\, dv. \quad (7) $$

The first advantage of using Beta distribution is that the random numbers generated by this distribution are always in the range of $[0, 1]$ which makes them perfect for the IBGAR method (see Figure 2). Moreover, we can easily control the skewness of the distribution by changing one or both parameters α and β.

Considering the explanations above, in low (high) incentives, the distribution should be right-skewed (left-skewed). So, to depend the skewness to the incentive, it is suggested that the β is kept as $\beta = \beta^0$ and represent the α as a function of normalized incentives as shown in Figure 4. When the incentive is low, i.e., the normalized incentive is close to -1, the assigned value for α should be much less than β^0. This increases the probability of generating random numbers close to 0, and sending access requests to the aggregator. When the normalized incentive is equal to 0, we should have $\alpha = \beta^0$ which gives a symmetric distribution for generating the random number. In this case, the probability of sending an access request would be 50%. In high incentives, i.e., normalized incentives close to 1, the assigned value for α is much greater than β^0. This yields the generation of random numbers close to 1, which means low probability of sending access requests.
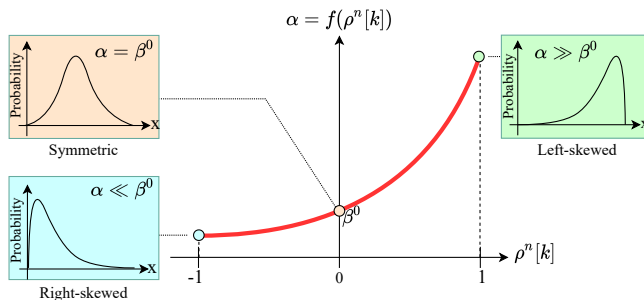

Figure 4: Illustrating the effects of α on skewness of the beta distribution and the relation between normalized incentive and α.

9

Different functions can be used to describe the relation between α and normalized incentives, i.e., $\alpha = f(\rho^n[k])$. The main feature of these functions is to be monotonically increasing by increasing the normalized incentive as depicted in Figure 4. In general, use of an exponential function as $\alpha = ae^{b\rho^n[k]}$ is suggested, where parameters $a \geq 0$ and $b \geq 0$ can be determined by choosing suitable values for α in normalized incentives -1, and 1, and noting that $f(0) = \beta^0$.

The process outlined above can be applied for all ranges of incentives including negative external incentives (e.g., negative prices as incentives). However, to add another lever to profit from negative incentives, it is suggested that parameter β^0 be replaced with β^{neg} where $\beta^{neg} \gg \beta^0$ for generating the random numbers in time intervals where the external incentive is negative. This will lead to generating random numbers very close to zero, and consequently, sending grid access requests for almost all values of the state variable inside the operational boundaries.

It is worth mentioning that according to (5) and (6), for flat incentive tariffs, we have $\rho^n[k] = 0 \ \forall k \in K$ and as shown in Figure 4, a symmetric distribution will be used to generate random numbers for all time intervals. So, IBGAR becomes independent of incentives. This is not a disadvantage to IBGAR because when a flat incentive is assigned, the incentive would be the same in all time intervals and consequently, will be removed from the decision-making process. The important point for keeping IBGAR efficient for flat incentive tariffs is that the amount of energy consumption in this method should not be more than energy consumption in the existing conventional control strategies. To solve this issue, the design parameter m_R introduced in (3) should be adjusted properly to reach a suitable energy consumption level for flat incentive tariffs.

2.1.3. Adding look-ahead capability to the method

As noted, look-ahead capability allows the device controller to include future variations in the boundary conditions of the state variable in the decision making. To add this feature to the method, it is suggested that the algorithm checks the changes in the boundary conditions in the next time intervals continuously, and to follow the below steps:

1. Recognize the next change in the boundary conditions and the time remaining to it (Δt_c),

2. Calculate the minimum time (t_{min}) required to meet the new boundary condition,

3. Compare t_{min} with Δt_c. If $t_{min} < \Delta t_c$ no change in the IBGAR method will be needed. If $t_{min} \geq \Delta t_c$, the opt out control should be used to temporarily exit the plan and control the device such that the lower/upper bound constraints are satisfied. An example of these two situations for the case where the lower bound changes in the next time intervals is illustrated in Figure 5.

It should be noted that it is not necessary to follow these steps in all cases where the boundary condition changes. Figure 6 illustrates all possible situations for changes in the boundary condition, the value of the state variable, and its possible realizations in the next hours. In cases (a) and (b), changes in the boundary conditions lead to increasing the feasible operating range. So it is not necessary to apply look-ahead capability. In cases (c) and (d) the feasible operating range reduces but the state variable is still inside the range of the next boundary conditions. So we can still postpone taking preventive
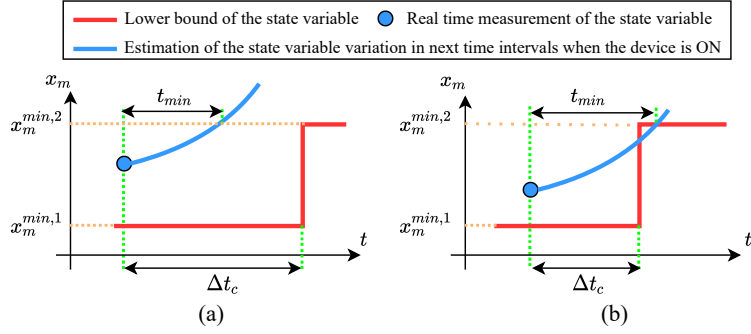
10

Figure 5: Illustration of two different situations for t_{min} and Δt_c, a) $t_{min} < \Delta t_c$ in which IBGAR can be followed b) $t_{min} \geq \Delta t_c$ in which opt out occurs.

actions. In cases (e) and (f), the feasible operating range reduces and if proper actions are not taken, the next boundary conditions may not be satisfied. So, the look-ahead capability should be applied only for cases (e) and (f).

Calculating t_{min} for each device and operation mode is different. For instance, for a battery, if the lower bound of SOC will increase in next time intervals, i.e. case (e) in Figure 6, then to obtain t_{min} we should assume charging the battery with maximum charging rate in the next time intervals and find the minimum time to meet the new lower bound as t_{min}. For a heating system, in case (e) the device should be ON and in case (f) the device should be OFF in the next time intervals and then dynamic model and experimental results should be used to find the minimum time to meet the new boundary condition as t_{min}. Detailed explanations about calculating t_{min} for the studied case will be presented in Section 3.

It is important to highlight that to include the look-ahead capability in this method, the rise time (or ramp-up/down times) need to be identified. In a practical implementation of IBGAR, this can be achieved with simple system identification or data analysis procedures on the physical assets without the need for precise mathematical models. Of course, for the simulation herein, we only need the thermodynamic model to estimate these parameters, but otherwise do not depend on exact models.

2.1.4. IBGAR algorithm at the device level

A block diagram of the proposed IBGAR algorithm for the device controller is presented in Figure 7. In the first step, the algorithm checks if applying look-ahead capability is required, i.e., the changes in the boundary condition and the value of the state variable
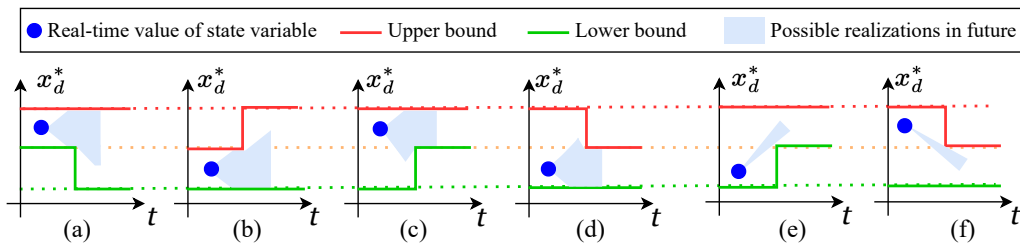

Figure 6: Different situations for the state variable and changes in the boundary condition: a,b,c,d) the look-ahead capability is not used, e,f) applying look-ahead capability.
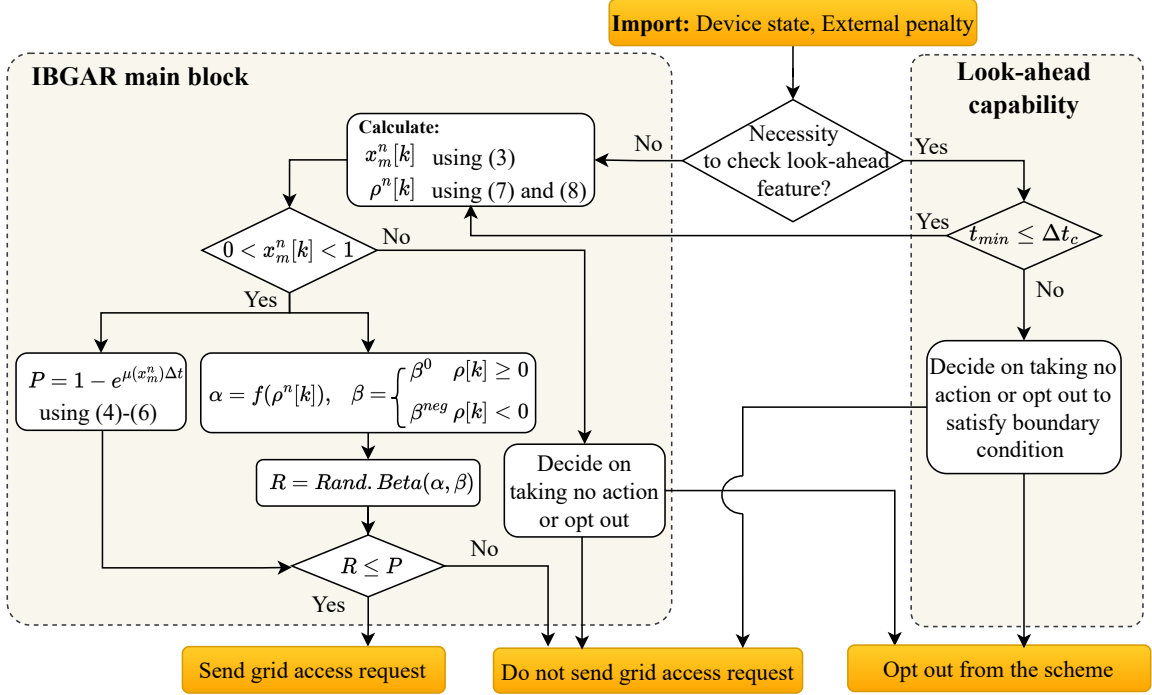
Figure 7: Block diagram of the proposed IBGAR at the device level.

are similar to cases (e) and (f) in Figure 6 or not. If yes, t_{min} and Δt_C are calculated (see section 2.1.3) and compared. As long as the state variable can satisfy the next boundary conditions, i.e., $t_{min} < \Delta t_C$, no specific action is needed and we can continue with IB-GAR main block, otherwise, considering the type of the device, one of the two actions a) opt-out and turning the device ON or b) not sending an access request and turning the device OFF should be taken. For instance, for a Heating (Cooling) device, if the lower bound is changing, the device should be ON (OFF) and if the upper bound is changing, the device should be OFF (ON) in the next time intervals.

In the next step, the algorithm checks if the normalized value of the state variable is between zero and one, i.e., inside the operation boundaries or not. If No, the algorithm decides on the opt-out from the program and turning the device ON or taking no action and turning the device OFF considering the type of the device, such that the state variable returns to the inside of the operating range as soon as possible. The last two steps can be considered as preprocessing steps to ensure QoS for the customer. If yes, two parameters P and R will be generated and compared. Parameter P represents the SRR function and depends on the state variable. Parameter R is a random number generated by Beta distribution while parameters of the distribution are controlled by the normalized incentive. If $R \leq P$, then the grid access request will be sent to the aggregator, otherwise, not.

The electricity demand of the device is also sent alongside the grid access request or opt-out signal to let the coordinator know the electricity consumption of the device. This could be the nominal power consumption of the device or the rated charging or discharging power of the batteries.

2.2. IBGAR method implementation at the coordinator level

As shown in Figure 1, the IBGAR method benefits from the possibility of bilateral data communication between devices and a coordinator (e.g., an aggregator) to provide flexibility services for the grid. At the coordinator level, the coordinator broadcasts the incentives, i.e., electricity price, CO_2 emission, etc., to devices. Then, each device decides whether to send or not send the access request to the coordinator. The coordinator receives access requests from devices and signals from the distribution system operator (DSO) or transmission system operator (TSO), and responds to the access requests using flexibility management system such that the error between the requested dispatch signal and its realization in the grid minimizes. A closed loop block diagram of the coordinator operation is depicted in Figure 8.
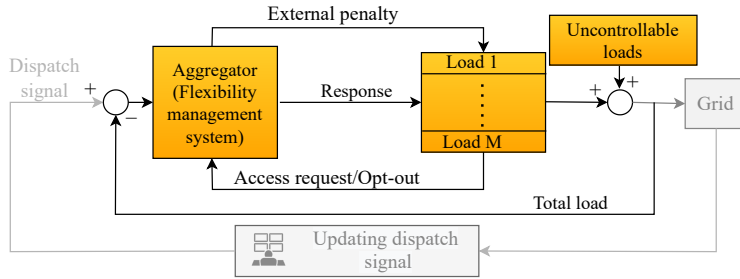
Figure 8: Closed loop block diagram of the aggregator operation for providing services at the distribution grid level.

One of the key elements in the effectiveness of the IBGAR scheme is designing the flexibility management system. Access request signals are sent in an asynchronous way, meaning that the access request signals of devices are received at different times. To send the responses back to devices, the flexibility management system waits for a time period δt (where $\delta t < \Delta t$), collects all the access requests received during this time interval and determines the "Yes" or "No" notification for each device based on the real-time error between actual aggregated output and the dispatch signal. Different approaches can be used to determine which access requests should be accepted among all requests received during the time interval δt. The first idea is to accept the requests sequentially. In this approach, the requests are prioritized based on the time received by the aggregator. This approach is simple but is not fair because if the Δt is the same for some devices, they will always be prioritized in a same way and some devices will always have higher priority over other devices. Another idea is to prioritize the requests based on the history of their requests in the last time intervals. In this approach, the devices with fewer requests in the last time intervals have higher priority to be supplied. This method is fair but more complicated than the first approach and more importantly due to recording the historical data, does not respect privacy. The third idea is to assign priorities randomly. This approach is fair, easy to implement, and respects privacy of end-users. Therefore, the third approach is used to prioritize the requests at each time interval δt.

It is worth noting that the actual implementation of PEM (as the basis of this work) shows that the communication delays for sending grid access requests are less than one second which is much smaller than the simulation time-steps Δt and δt and does not affect the simulation results significantly [28] [29]. Moreover, to preserve privacy, the coordinator

receives grid access requests anonymously and accepting or rejecting the requests does not require any knowledge/tracking of a particular device.

3. Case study and numerical results

Among different controllable devices, heat pumps that are used to supply swimming pools are found to be ideal flexibility resources in many studies due to the high thermal storage capacity of the pools [30] [31] [32]. In Denmark, the NOVASOL company manages more than 900 summerhouses with indoor swimming pools that are mostly heated by heat pumps [32]. Moreover, the incorporation of other controllable devices such as batteries and EVs into the PEM method has already been investigated [22],[33]. So, we focus on a test system with swimming pool heating systems (SPHSs) supplied by heat pumps as controllable loads and some uncontrollable loads as the case study. In order to show how the method works at the aggregator level, it is assumed that the loads in the area are supplied through a transformer with limited rated active power. The aggregator receives the flexibility request signal from a DSO to use flexibility such that the transformer does not get overloaded. Other services such as frequency control or voltage regulations can also be provided by the aggregator, however, the approach in the aggregator and device levels would be the same.

Figure 9 provides a schematic representation of a heat pump and swimming pool set-up. In [34] a gray-box model is proposed to model the dynamics of this SPHS. Parameters of this gray-box model are used as the basis to describe the dynamics of the studied SPHSs in this work. In order to obtain data for large number of SPHSs, it is suggested that some realistic scenarios are generated for each parameter, taking into account the calculated values in [34], and then use different combinations of these scenarios as input data for each SPHS. Table 2 represents related scenarios for each parameter. Using these scenarios, 35 sets of data are generated to represent 35 SPHSs for the studied system.
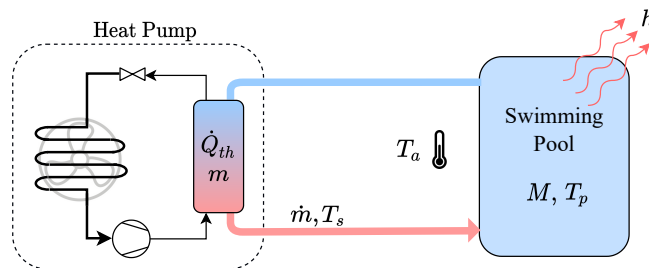
Figure 9: Schematic representation of heat pump and swimming pool set-up [35].

Table 2: Scenarios used for generating SPHSs parameters

$M_d(kg)$	$m_d(kg)$	$\dot{m}_d(kg/h)$	$P_d^n(kW)$
30000	$\{2100, 3900\}$	$\{4350, 5900\}$	$\{7, 5, 3\}$
40000	$\{2800, 5200\}$	$\{5900, 7900\}$	$\{9, 6, 4\}$
50000	$\{3500, 6500\}$	$\{7900, 9800\}$	$\{11, 8, 5\}$

Parameters $M_d(kg)$, $m_d(kg)$ and $\dot{m}_d(kg/h)$ are the mass of water in the pool and heat exchanger and the flow rate for outlet water from the heat exchanger, respectively.

$P_d^n(kW)$ is the rated power of the heat pump. Since the studied cases are indoor pools, it is assumed that the ambient temperature does not change significantly during the day and varies between $17°C$ and $20°C$. The heat transfer coefficient of the pool, $h(kW/K)$, is assumed to be the same for all SPHSs and equal to $0.5\ kW/K$.

Electricity price is considered as the external incentive. Both dynamic and flat price tariffs are investigated. Elspot market prices for the DK1 grid region (west Denmark) in January 2022 plus a fixed tariff are chosen as dynamic electricity price inputs [36]. Flat tariff price is assumed to be equal to the average dynamic prices. The load of the DK1 grid region in January 2022 is scaled to obtain the data for aggregated electricity consumption by uncontrollable loads in the studied test system.

At each pool, the water temperature should follow a set-point. A dead-band (upper and lower bounds) is defined around the set-point that limits the temperature variations around the set-point. Without loss of generality, it is assumed that the upper bound is constant but the lower bound can change over time as the set-point changes by users. It is assumed that changes to the boundary conditions occur at predetermined times (e.g., based on scheduled occupancy). Δt and δt are assumed to be 20 min and 100 sec, respectively.

As discussed before, the IBGAR method implementation does not depend on a mathematical model of the devices and the decisions can be made based on the real-time measurements of the studied case and the external incentive. Even for implementing the look-ahead capability, we can replace the mathematical model of the system with some preheating tests performed before executing the method. However, to have a simulation-based study, a discrete-time model is needed to estimate the variation of the state variable at each time interval. Moreover, in case the system has time-varying boundary conditions, a simple model of the system will be useful for including the look-ahead capability in the method (see section 2.1.3. In Appendix A a general description of the process of obtaining a discrete-time model of a control device followed by the discrete-time model of the SPHSs is presented. This model is used in this paper to model the dynamics of SPHSs.

3.1. Designing the parameters a and b in $f(\rho^n[k])$ and m_R

As mentioned in Subsection 2.1.2, variable α in the beta distribution is determined as a function of normalized price i.e., $\alpha = f(\rho^n[k]) = ae^{b\rho^n[k]}$. To obtain parameters a and b, first, values of function f for $\rho^n[k] = -1, 0, 1$ are determined, and then a curve fitting tool such as *cftool* in MATLAB is used to estimate a and b.

For $\rho^n[k] = 0$, as discussed in Section 2.1.2, we should have $f(0) = \beta^0$ to have symmetric probability distribution for generating random numbers when the tariff is flat or equal to the average price of the day. It is assumed that $f(\rho^n[k] = -1) = 1$ which provides enough right skewness for the Beta distribution when prices are very low. We also take $f(\rho^n[k] = 1) = (\beta^0)^2$. This provides enough non-linearity in the function f and consequently enough left skewness in the Beta distribution that significantly reduces the rate of sending grid access requests at high prices. So, the three sets of data points will be as $(-1, 1)$, $(0, \beta^0)$ and $(1, (\beta^0)^2)$, which highlights the key role of β^0 in designing the parameters a and b. To find a suitable value for β, we need to run the simulations for its different values and evaluate the results. However, to run the simulations, we should also determine the design parameter m_R in (3) and (4). Since both β and m_R affect the outputs, simulations are performed for different values of both parameters and then, by

analyzing the results and using cost and comfort-related metrics, suitable values of these parameters will be found.

Electricity cost reduction compared to conventional methods is used as the cost-related metric. Most existing SPHSs work with the conventional binary ON/OFF method. In this method, the SPHS is controlled to follow a set-point temperature T_d^{set} within the lower ($T_d^{min}[k]$) and upper ($T_d^{max}[k]$) bounds of water temperature which can be expressed mathematically as follows:

$$u_m[k] = \begin{cases} 1 & T_d^p[k] < T_d^{min}[k], \\ 0 & T_d^p[k] > T_d^{max}[k] \ . \\ u_m[k-1] & \text{Otherwise} \end{cases} \tag{8}$$

Percentage of mean normalized temperature deviation (MNTD) from set-points for all pools are defined as the metrics related to users' comfort. MNTD is formulated as below:

$$MNTD = \frac{1}{NK} \sum_{d=1}^{N} \sum_{k=1}^{K} \frac{T_d^p[k] - T_d^{set}[k]}{T_d^{max}[k] - T_d^{min}[k]}, \tag{9}$$

The percentage of variations in the electricity cost of SPHSs compared to the conventional ON/OFF method and variations in the MNTD compared to the set-point temperatures for different values of β and m_R and for both dynamic and flat price tariffs are presented in Figure 10.
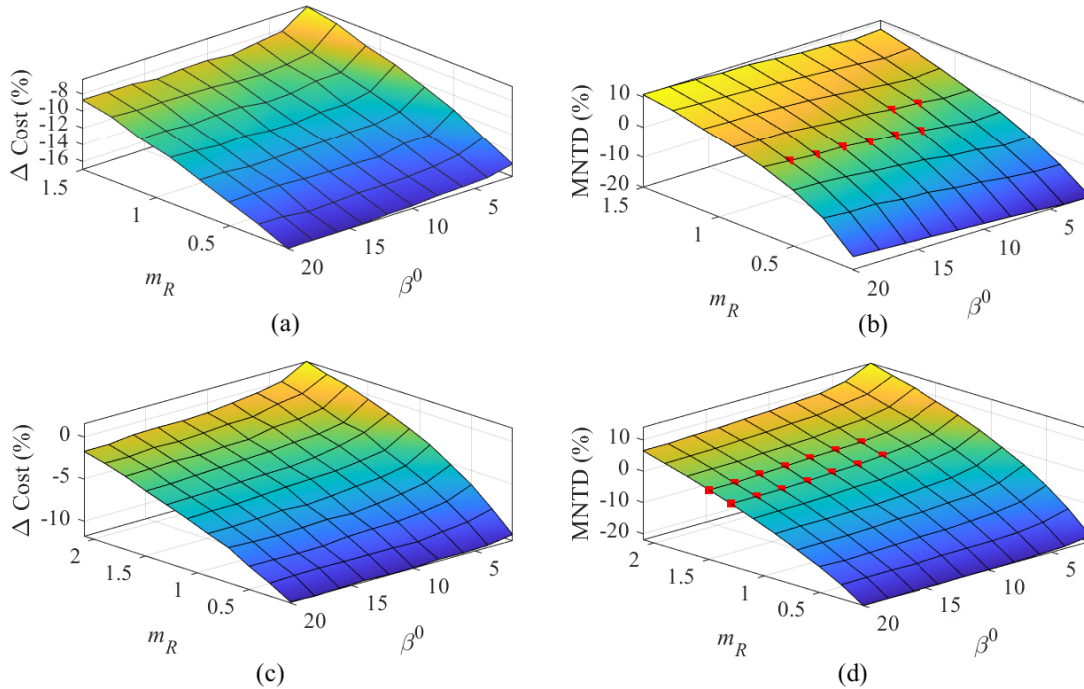
Figure 10: Impacts of β and m_R on a) electricity cost and b) MNTD for dynamic tariffs and c) electricity cost and d) MNTD for flat tariffs.

As shown in Figure 10a, for dynamic tariffs, by increasing β^0, electricity cost decreases. This happens due to the inverse relationship between β and the variance of the Beta

distribution. For small values of β, the variance of the distribution is high, which increases the possibility of generating undesirable random numbers and consequently increasing the cost. For $\beta^0 \geq 6$, the impact of β on cost is not significant and the cost is almost constant. Increasing m_R increases both cost and MNTD due to its direct relationship with the rate of grid access requests (see Figure 3). So, overall, from the cost-effectiveness perspective, we should have $\beta^0 \geq 6$, however, if we wanted to keep the mean temperature close to the set points we should choose pairs of $\beta^0 \geq 6$ and m_R that lead to MNTDs close to zero. Some examples of these values are highlighted in 10b in red. Among these points, the ones with lower m_R values are more preferable due to their impacts on decreasing the cost. So, for dynamic tariffs, it is suggested to have $m_R = 0.7$ and $\beta^0 \geq 8$. Following the same procedure for flat tariffs, we should have $m_R = 1.3$ and $\beta^0 \geq 8$.

Figure 10 also shows that the operation cost and temperature variation in the studied system are more affected by parameter m_R than β^0.

It is worth mentioning that considering different values for β^0 and m_R, the temperature will always be inside the dead-band (between the lower and upper bound). Choosing different values for these parameters helps us to manage the temperature variations inside the dead-band such that it fluctuates around the set-point or close to the lower and upper bounds. Water temperature variation of an arbitrary pool in the studied system for three different values of β^0 and m_R are presented in Figure 11. The look-ahead capability which will be discussed in Section 3.2 is also included in the simulations.
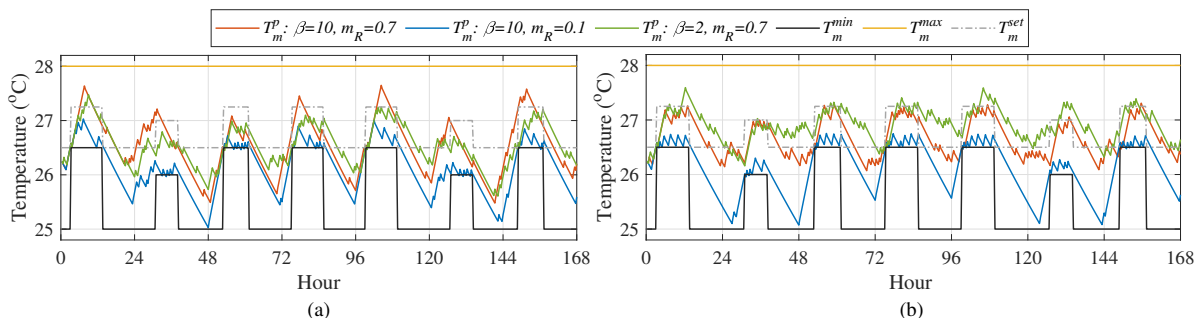

Figure 11: Water temperature variations in three different cases for a) dynamic tariffs and b) flat tariffs.

As shown in Figure 11a, for dynamic price tariffs, when $m_R = 0.1$, the water temperature is lower than other cases and is usually close to the lower bound, specially when the lower bound increases. In the case that $m_R = 0.7$ and $\beta^0 = 10$, the temperature tries to follow the set-point considering the electricity price. When $\beta^0 = 2$ and $m_R = 0.7$, in comparison to the case that $\beta^0 = 10$ and $m_R = 0.7$, the temperature is usually lower, but the electricity cost is about 7% higher. As discussed before in this section, this is due to high variance of the beta distribution when β^0 is small and consequently generating undesirable random numbers.

For flat price tariff, similarly, the temperature is the lowest when $m_R = 0.1$. However, when $m_R = 1.3$ and $\beta^0 = 10$ the method is more successful in following the set-point than the case with dynamic tariffs. This happens because for flat price tariffs, the method is not dependent on price and only tries to follow the set-point. It can also be seen in Figure 11b that when $\beta^0 = 2$ and $m_R = 1.3$ the method is not successful in following

17

the set-point and the temperature is usually more than the temperature of the case that $\beta^0 = 10$ and $m_R = 1.3$.

In the rest of the paper, we have $\beta^0 = 10$ and $m_R = 0.7$ for dynamic tariffs and $\beta^0 = 10$ and $m_R = 1.3$ for flat tariffs. This results in 13% and 5% reduction in electricity cost by using the IBGAR method with dynamic and flat tariffs, respectively.

3.2. Look-ahead capability feature modeling

As discussed at the beginning of this section, it is assumed that only the lower bound of temperature changes over the time. In this case, we can consider the look-ahead capability as a part of the "preheating process". As mentioned in Section 2.1.3, to incorporate this process, we need to compute the parameter t_{min} that represents the minimum time for increasing the temperature up to the next lower bound. For an SPHS, this parameter can be calculated by solving the differential equations (A.3) and (A.4). Solving these equations gives $T_d^p(t)$ as below:

$$T_d^p(t) = A_d + B_d e^{\tau_d^1 t} + C_d e^{\tau_d^2 t}. \tag{10}$$

Parameters A_d, B_d, C_d, τ_d^1, and τ_d^2 are defined in Appendix B. Obtaining a closed-form expression for t_{min} from (10) is non-trivial. However, considering (B.1) and (B.2) in Appendix B and SPHSs data presented at the beginning of Section 3 and Table 2, it can be seen that the term $\frac{\dot{m}_d h'}{M_d m_d}$ is very small which leads to $\tau_d^2 \ll \tau_d^1$. So, we can simplify the equation as below:

$$T_d^p(t) \approx A_d + C_d e^{\tau_d^2 t}. \tag{11}$$

Figure 12a compares the variations in the pool water temperature using (10) and (11) for an arbitrary SPHS. It can be seen that applying the simplification causes error only in the first hour and then the error is zero. Since the goal of using look-ahead capability is to estimate the temperature in the next few hours, this error will not affect the results. Now, using (11), t_{min} can be easily estimated as following:
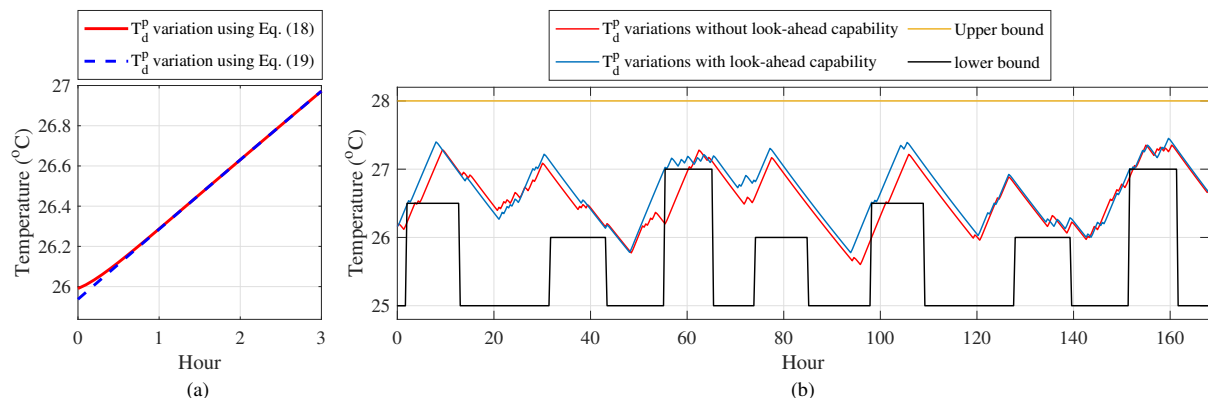

Figure 12: Impacts of a) simplifying Eq. (10) on temperature variation modeling, and b) applying look-ahead capability to the model.

$$t_{min} \approx \frac{ln(\frac{T_d^{min,2} - A_d}{C_d})}{\tau_d^2}, \tag{12}$$

18

where $T_d^{min,2}$ is the next lower bound for the pool temperature. Figure 12b illustrates the impacts of including the preheating process on the reaction in changing the lower bound temperature for an SPHP. As shown in Figure 12b, taking into account the look-ahead capability prevents the temperature from falling below the lower bound in all situations.

3.3. Implementing the IBGAR method without including the transformer limitations

In this section, the impacts of the proposed method on responding to dynamic and flat tariffs are studied. To investigate the responsiveness of the method to dynamic prices, consumed power by SPHSs and prices are depicted in Figure 13. It can clearly be seen that using the IBGAR method electricity consumption is shifted mostly to low electricity price hours, which confirms the price responsiveness of the method.
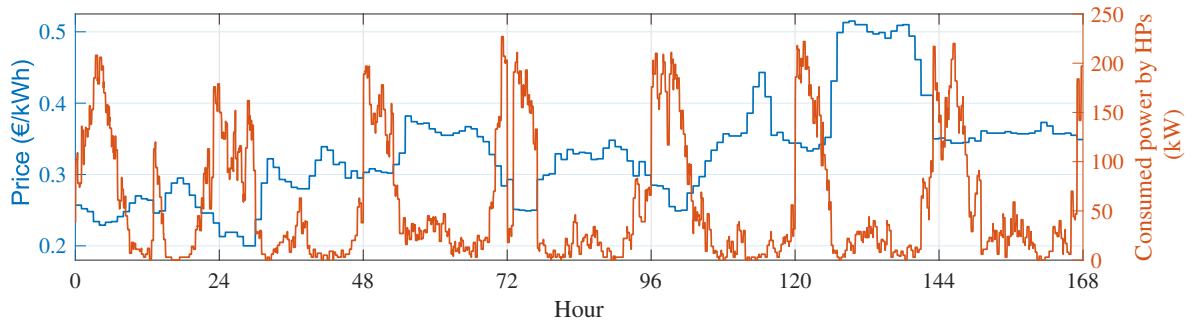
Figure 13: Comparing the power consumption of the SPHSs and electricity price.

Power consumption of the set of all controllable and uncontrollable loads for both traditional and the IBGAR methods with dynamic and flat tariffs is presented in Figure 14.

As it can be seen in Figure 14, using the proposed IBGAR method can reduce the peak demand and the gap between maximum and minimum load (help to flatten the demand curve). Numerical details are presented in Table 3.
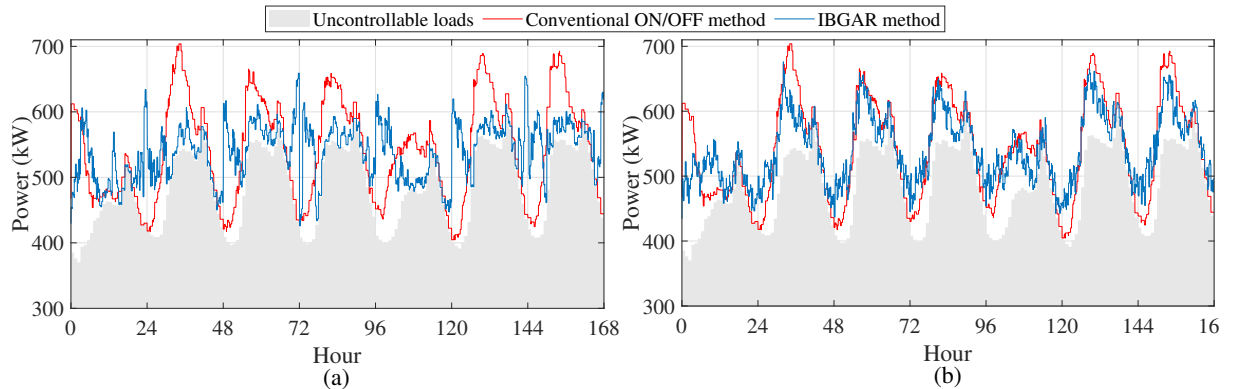

Figure 14: Comparing the total power consumption of the traditional ON/OFF method with a) dynamic tariffs and b) flat tariffs.

Table 3: Impacts of the proposed method in reducing the peak load and the gap between maximum and minimum load compared to the traditional method.

	Dynamic tariff	Flat tariff
Reduction in peak load	7 %	3.8 %
Reduction in the gap between maximum and minimum load	24 %	20 %

3.4. Implementing the IBGAR method including the transformer limitations

Figure 15 illustrates the impacts of considering transformer limitations on the aggregator's response to grid access requests and consequently total load. The number of rejected requests when the price tariff is flat is much more than the case with dynamic tariff because of higher electricity consumption of the IBGAR method with flat tariffs. In case of using a dynamic tariff, rejected requests mostly belong to off-peak hours and then mid-peak hours. This happens because in on-peak hours, there are the least access requests and hence, the number of rejected requests is very low. In off-peak hours, the number of requests is very high which in some cases may cause rejecting some grid access requests. During the mid-peak hours, the available capacity is less than off-peak hours and the number of access requests is more than on-peak hours, which leads to rejection of some of the requests. Using flat tariffs, all rejected requests occur in mid-peak and on-peak hours because power consumption of controllable devices does not decrease at these hours and their aggregation with high demand of uncontrollable loads in mid-peak and on-peak hours leads to violating the transformer rate power.

As illustrated in Figure 15, there are some time intervals, e.g., hour 137 for dynamic tariffs and 128, 130, and 132 for flat tariffs, where the aggregator cannot keep the total load below the rated active power of the transformer. This is due to the opt-out possibility defined for devices to satisfy their boundary conditions.

Remark: Clearly, there is a trade-off between guaranteeing comfort (QoS) at the device level and guaranteeing grid constraints/reliability. That is, if we enforce the grid constraint (and remove opt-outs), then we cannot guarantee QoS. Thus, there is a fundamental limitation with any coordination scheme to either preserve grid limits or QoS. Herein, we have prioritized device QoS since small, short-duration power overloads (as illustrated herein) do not significantly impact transformer operations or winding insulation [37]. In addition, by actively managing device QoS via IBGAR, we exactly avoid large demand spikes that could result from coincident opt-outs and cause larger power overloads.

3.5. Impacts of negative electricity prices on the results

Negative prices can happen during the off-peak hours when electricity consumption is low due to technical limitations of power generators or excess output power of renewable resources. To study the impacts of negative prices on the results, simulations are repeated for two cases, 1) normal daily prices, 2) assigning negative prices for some hours of a day. Transformer limitations are not taken into account and the focus is only on the role of negative prices in energy consumption and water temperature variations. Simulations are performed for two days and it is assumed that negative prices are applied during the first
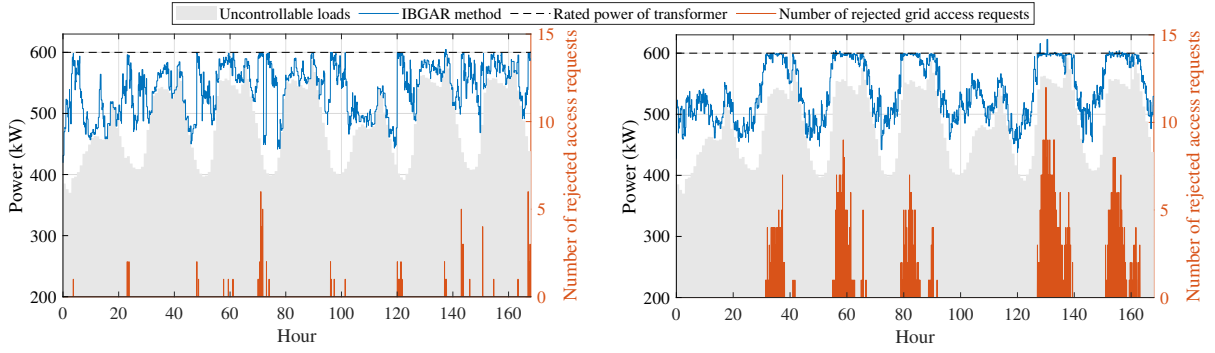
Figure 15: Power consumption of the loads and number of rejected grid access requests by the aggregator taking into account the transformer limitations for a) dynamic price tariffs and b) flat price tariffs.
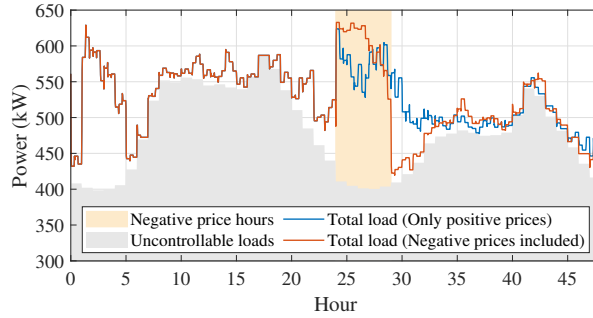

Figure 16: Impacts of including negative prices on the total power consumption of the test system.

five hours of the second day (hours 24 to 29). Total consumed power of the test system is presented for both cases in Figure 16.

It can be seen that by applying negative prices, at first, the power consumption of the test system increases as expected, and then decreases from hour 27 (3:00 a.m. of the second day) due to the water temperatures of some swimming pools reaching their maximum values. After hour 29, the power consumption decreases significantly, because the water temperature of the pools is high and hence, there will be less need for energy consumption in the next hours (rebound effect).

Water temperature variations in three arbitrary pools are presented in Figure 17. In Figure 17.a, the heat pump is ON during the negative price hours, reaches the upper limit at the end of the negative price hours period and then it will be OFF for the rest of the day. In Figure 17.b, the heat pump is ON in the first four hours, then it reaches to the maximum temperature and will be OFF for some time intervals, and finally turns ON again before the negative price hours period ends to benefit from negative prices. The heat pump in Figure 17.c has a slow dynamic and while the heat pump is ON during the negative price hours period, the temperature does not reach the maximum value. After the negative price hours period, since the normalized prices in case 2 are greater than normalized prices in case 1 (due to including negative prices in (5) and (6)), fewer grid access requests will be sent, and hence, the temperature will be lower than the temperature in case 1. However, the operational constraints are still satisfied.
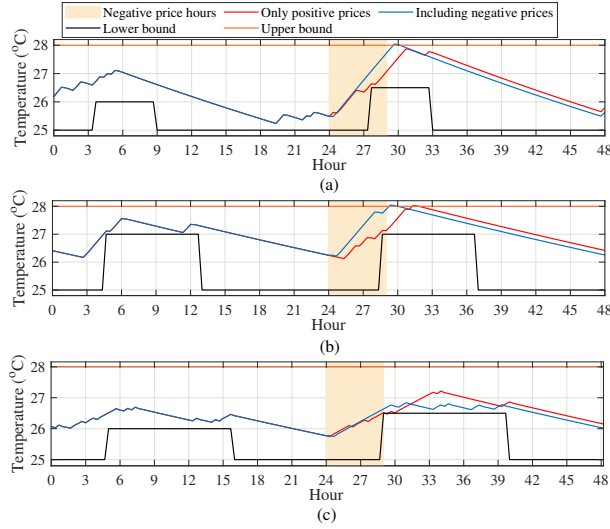
Figure 17: Impacts of including negative prices on the temperature variations in swimming pools a) 1, b) 7, and c) 15.

3.6. A comparative analysis among different approaches

In this section, the proposed IBGAR method is compared with the traditional ON/OFF method and the standard PEM method from the perspective of operation cost, energy consumption, and deviation from set point temperature (MNTD). Price tariff is assumed to be dynamic. To model the standard PEM method, the impact of external incentives on generating random numbers in the ARM (see Figure 2) is ignored and the uniform distribution is used to generate random numbers. Despite the proposed IBGAR method, both the traditional method and the standard PEM method cannot take into account the look-ahead capability. Simulation results are presented in Table 4. It can be seen that using the proposed method the lowest electricity cost would be achieved compared to the other two methods. The absolute value of deviations from the reference temperature in the IBGAR method is also less than other methods. However, more energy is consumed compared to the PEM method. This is due to high energy consumption in low-price hours.

Table 4: Comparing the simulation results of the proposed IBGAR method with the traditional method and the PEM.

	Electricity cost (€)	Energy consumption (kWh)	MNTD (^{o}C)
Traditional method	3185.5	9719.1	0.0908
PEM method	3001.3	9401.5	-0.1447
IBGAR method	2860.6	9582.8	-0.0228

3.7. Sensitivity analysis on the number of controllable devices

To understand the improvements of the IBGAR method compared to the PEM regarding the capability of including controllable devices, in this section, a sensitivity analysis is performed on the number of devices. To this end, the number of devices varies between 5

and 70, and simulations are repeated for each group of devices. The goal is to see how the number of rejected grid access requests and transformer loading is affected by choosing IBGAR or the PEM method. Simulation results for dynamic price tariffs and for the studied time period in section 3.4 are presented in Figure 18. It can be seen that the IBGAR gives a better performance in all defined factors, i.e., 1) the number of rejected requests, 2) maximum violations from transformer limitations, and 3) energy transformed beyond the nominal capacity of the transformer. For PEM, rejection of requests starts from 20 devices, while the same happens for IBGAR when the number of devices is 35. When the number of devices is 45, the number of rejected requests for IBGAR is almost 1800 less than the PEM. While the maximum violation from transformer limitation in the IBGAR method with 45 devices is $4kW$ this number is $39kW$ for the PEM. The energy transformed beyond the capacity of the transformer is not significant up to 55 devices for the IBGAR method. This number is 40 devices for the PEM method.

It can also be seen that when the number of devices is very high the two methods show similar results. This is because, at this number of devices, the transformer is overloaded almost all the time, and hence there is not much flexibility in operation and the two methods tend to each other.
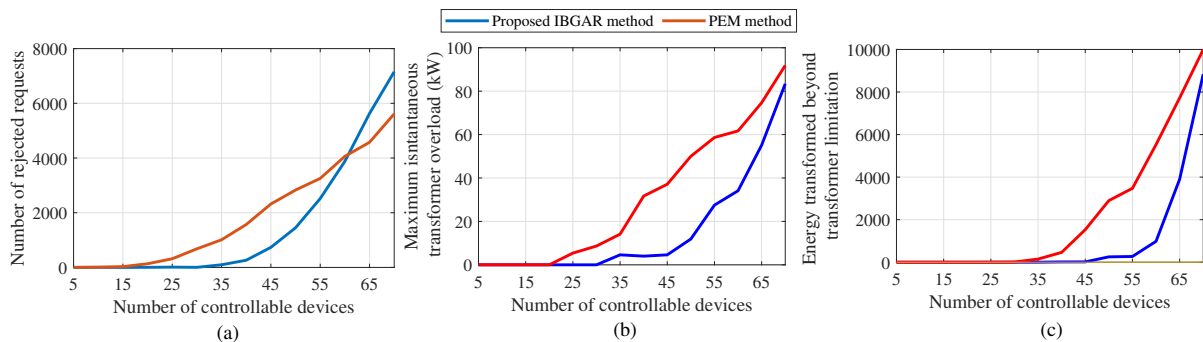

Figure 18: Sensitivity analysis on the number of controllable devices.

4. Conclusion

In this work, a coordination method for procuring the flexibility of controllable devices is proposed. The method works based on sending incentive-based randomized grid access requests from controllable devices to an aggregator and receiving "Yes" or "No" notifications. Grid access requests are generated through a stochastic process in which price-dependent random numbers are evaluated by a stochastic rate request function to decide about sending or not sending the grid access request. The devices are also allowed to opt out of the program temporarily and keep the device ON to satisfy their operational constraints.

The main features of the proposed method are bottom-up structure for providing flexibility that ensures customers' quality of service, respecting the privacy of end-users, low computational complexity which leads to less need for powerful hardware and thus cheaper installation costs, and being model-free in many applications that increases the chance of its large-scale implementation. The method can be applied to any deferrable loads that controlling it for a limited time interval (Δt) does not violate its technical limitations and customers' comfort.

The simulation results show that the method is suitably price responsive and compared to conventional methods, it can decrease the electricity costs up to 17% and 11% for dynamic and flat price tariffs, respectively. The method is also capable of dealing with time varying boundary conditions, however, due to look-ahead implementations, this element requires a (simplified) model of the devices' responses. The effectiveness of the method in dealing with negative prices is also investigated. At the system level, the proposed method is useful for peak shaving and load curve flattening. Simulation results highlights the effectiveness of the proposed method in providing energy and grid ancillary services by aggregators while respecting the operational constraints of the devices.

Future directions of this work could include combining the method with other incentive-based approaches (e.g., flexibility functions), enhancing the grid-awareness capabilities of the method, incorporating more detailed operational models of heat pumps to account for part-load operations and efficiency, extending the method to other controllable devices, using more advanced methods for calculating the design parameters such as machine learning and upgrading the method to allow sending analog requests (such as the availability level) instead of binary request/no request signals.

Appendix A. Controllable device modeling

The differential equations of state variables for controllable device d can be formulated as below:

$$\frac{dX_d(t)}{dt} = A_d X_d(t) + B_d U_d(t) \tag{A.1}$$

where $X_d^{a \times 1}$ and $U_d^{b \times 1}$ are the vectors of state variables and inputs, and $A_d^{a \times a}$ and $B_d^{a \times b}$ are state and input matrices, respectively. a and b refer to the number of state variables and inputs, respectively. An approximate discrete-time representation of (A.1) in $t \in [k\Delta t, (k+1)\Delta t]$ is obtained as below:

$$X_d[k+1] = (I + A_d \Delta t) X_d[k] + B_d U_d[k] \Delta t \tag{A.2}$$

where $I^{a \times a}$ is an identity matrix. Using (A.2), we can update the state variables at the end of each time interval.

For a SPHS as the studied case the thermodynamic model of the SPHS d is formulated by the two following equations [32]:

$$m_d c_p \frac{dT_d^s(t)}{dt} = \dot{m}_d c_p (T_d^p(t) - T_d^s(t)) + \dot{Q}_d^{th}(t), \tag{A.3}$$

$$M_d c_p \frac{dT_d^p(t)}{dt} = \dot{m}_d c_p (T_d^s(t) - T_d^p(t)) + h(T_d^a(t) - T_d^p(t)). \tag{A.4}$$

Equation (A.3) gives the power balance in the heat exchanger. $T_d^s(^oC)$ and $T_d^p(^oC)$ are the supply and pool water temperatures, respectively. T_d^p is chosen as the state variable for IBGAR algorithm for SPHS d. $c_p(kj/kgK)$ is the specific heat capacity of water. $\dot{Q}_d^{th}(kW)$ is the thermal power received from the heat pump and can be obtained as below:

$$\dot{Q}_d^{th}(t) = P_d^n \times u_d(t) \times COP_d(t), \tag{A.5}$$

where u_d is a binary control input that refers to the ON/OFF status of heat pump d. The coefficient of performance (COP) gives the relationship between the power that is drawn out of the heat pump and the power that is supplied to the heat pump as:

$$COP_d(t) = \frac{T_d^h(t) + 273}{T_d^h(t) - T_d^a(t)} \eta_d^H, \tag{A.6}$$

where $T_d^h(^oC)$ is the condenser temperature, $T_d^a(^oC)$ is the ambient temperature above the pool, and η_d^H is the second-law efficiency and assumed to be equal to 0.4.

Equation (A.4) gives the power balance of the pool. Discrete-time model of equations (A.3) and (A.4) are used to obtain an estimation of water temperature variation such that $u_d(t) := u_d[k]$ for $t \in [k\Delta t, (k+1)\Delta t]$, as below:

$$T_d^s[k+1] = (1 - \frac{\dot{m}_d\Delta t}{m_d})T_d^s[k] + \frac{\dot{m}_d\Delta t}{m_d}T_d^p[k] + \frac{P_d^n\Delta t}{m_d c_p}COP_d[k]u_d[k], \tag{A.7}$$

$$T_d^p[k+1] = \frac{\dot{m}_d\Delta t}{M_d}T_d^s[k] + (1 - \frac{\dot{m}_d\Delta t}{M_d} - \frac{h\Delta t}{M_d c_P})T_d^p[k] + \frac{h\Delta t}{M_d c_p}T_d^a[k]. \tag{A.8}$$

Equations (A.7) and (A.8) are used to update the water temperature of the pool after each time interval in the simulations.

Appendix B. Defining the parameters of equations (10)

To calculate parameters A_d, B_d, C_d, τ_d^1, and τ_d^2 in (10), the differential equations (A.3) and (A.4) should be solved. To do this, first, the equivalent Laplace transform of these equations are written. Then, by solving these two equations, we can find $T_d^p(s)$ as a function of $u_d(s)$, $T_d^a(s)$, and initial conditions $T_d^p(0)$ and $T_d^s(0)$. Afterwards, by finding the inverse Laplace transform of the $T_d^p(s)$, $T_d^p(t)$ can be found as (10). Following the steps above, parameters τ_1, τ_2 A_d, B_d, and C_d, are obtained as below:

$$\tau_d^1 = -\frac{(M_d\dot{m}_d + m_d(\dot{m}_d + h'))}{2M_dm_d} - \sqrt{(\frac{M_d\dot{m}_d + m_d(\dot{m}_d + h')}{2M_dm_d})^2 - \frac{\dot{m}_dh'}{M_dm_d}}, \quad \text{(B.1)}$$

$$\tau_d^2 = -\frac{(M_d\dot{m}_d + m_d(\dot{m}_d + h'))}{2M_dm_d} + \sqrt{(\frac{M_d\dot{m}_d + m_d(\dot{m}_d + h')}{2M_dm_d})^2 - \frac{\dot{m}_dh'}{M_dm_d}}, \quad \text{(B.2)}$$

$$A_d = T_d^a + \frac{P_d^n COP_d}{h}, \quad \text{(B.3)}$$

$$B_d = \frac{P_d^n COP_d\dot{m}_d/c_p + \dot{m}_dh'T_d^a + (m_dh'T_d^a + M_d\dot{m}_dT_d^p(0) + m_d\dot{m}_dT_d^s(0))\tau_d^1 + M_dm_dT_d^p(0)(\tau_d^1)^2}{M_dm_d\tau_d^1(\tau_d^1 - \tau_d^2)},$$

$$\text{(B.4)}$$

$$C_d = \frac{P_d^n COP_d\dot{m}_d/c_p + \dot{m}_dh'T_d^a + (m_dh'T_d^a + M_d\dot{m}_dT_d^p(0) + m_d\dot{m}_dT_d^s(0))\tau_d^2 + M_dm_dT_d^p(0)(\tau_d^2)^2}{M_dm_d\tau_d^2(\tau_d^2 - \tau_d^1)},$$

$$\text{(B.5)}$$

where $h' = \frac{h}{c_p}$.

References

[1] F. D'Ettorre, M. Banaei, R. Ebrahimy, S. A. Pourmousavi, E. Blomgren, J. Kowalski, Z. Bohdanowicz, B. Łopaciuk Gonczaryk, C. Biele, H. Madsen, Exploiting demand-side flexibility: State-of-the-art, open issues and social perspective, Renewable and Sustainable Energy Reviews 165 (2022) 112605. doi:https://doi.org/10.1016/j.rser.2022.112605.

[2] M. Banaei, F. D'Ettorre, R. Ebrahimy, E. M. V. Blomgren, H. Madsen, Mutual impacts of procuring energy flexibility and equipment degradation at the residential consumers level, in: 2021 IEEE PES Innovative Smart Grid Technologies Europe (ISGT Europe), 2021, pp. 1–6. doi:10.1109/ISGTEurope52324.2021.9640142.

[3] E. M. V. Blomgren, R. Ebrahimy, A. Pourmousavi Kani, J. Kloppenborg Moller, F. D'Ettorre, M. Banaei, H. Madsen, Behind-the-meter energy flexibility modelling for aggregator operation with a focus on uncertainty, in: 2021 IEEE PES Innovative Smart Grid Technologies Europe (ISGT Europe), 2021, pp. 1–6. doi:10.1109/ISGTEurope52324.2021.9640146.

[4] D. Bertsekas, J. Tsitsiklis, Parallel and Distributed Computation: Numerical Methods, Prentice Hall Englewood Cliffs, NJ, vol. 23., 1989.

[5] L. M. Torriti J, Mohamed GH, Demand response experience in europe: Policies, programmes and implementation, Energy 35 (2010) 1575–1583.

[6] R. S. Montrose, J. F. Gardner, A. C. Satici, Centralized and decentralized optimal control of variable speed heat pumps, Energies 14 (13) (2021).

[7] M. Song, C. Gao, M. Shahidehpour, Z. Li, J. Yang, H. Yan, State space modeling and control of aggregated tcls for regulation services in power grids, IEEE Transactions on Smart Grid 10 (2019) 4095–4106.

[8] S. H. Tindemans, V. Trovato, G. Strbac, Decentralized control of thermostatic loads for flexible demand response, IEEE Transactions on Control Systems Technology 23 (5) (2015) 1685–1700. `doi:10.1109/TCST.2014.2381163`.

[9] Y. Wan, C. Long, R. Deng, G. Wen, X. Yu, T. Huang, Distributed event-based control for thermostatically controlled loads under hybrid cyber attacks, IEEE Transactions on Cybernetics 51 (11) (2021) 5314–5327. `doi:10.1109/TCYB.2020.2978274`.

[10] J. Arroyo, S. Gowri, F. De Ridder, L. Helsen, Flexibility quantification in the context of flexible heat and power for buildings, in: Proceedings of the Federation of European Heating, Ventilation and Air Conditioning associations conference, 2018, brussels, Belgium.

[11] S. K. Gupta, T. Ghose, K. Chatterjee, Coordinated control of incentive-based demand response program and bess for frequency regulation in low inertia isolated grid, Electric Power Systems Research 209 (2022) 108037. `doi:https://doi.org/10.1016/j.epsr.2022.108037`.

[12] W. Zheng, D. J. Hill, Incentive-based coordination mechanism for distributed operation of integrated electricity and heat systems, Applied Energy 285 (2021) 116373. `doi:https://doi.org/10.1016/j.apenergy.2020.116373`.

[13] M. Yu, S. H. Hong, Y. Ding, X. Ye, An incentive-based demand response (dr) model considering composited dr resources, IEEE Transactions on Industrial Electronics 66 (2) (2019) 1488–1498. `doi:10.1109/TIE.2018.2826454`.

[14] H. Zhong, L. Xie, Q. Xia, Coupon incentive-based demand response: Theory and case study, IEEE Transactions on Power Systems 28 (2) (2013) 1266–1276. `doi:10.1109/TPWRS.2012.2218665`.

[15] R. G. Junker, A. G. Azar, R. A. Lopes, K. B. Lindberg, G. Reynders, R. Relan, H. Madsen, Characterizing the energy flexibility of buildings and districts, Applied Energy 225 (2018) 175–182. `doi:https://doi.org/10.1016/j.apenergy.2018.05.037`.

[16] R. G. Junker, C. S. Kallesøe, J. P. Real, B. Howard, R. A. Lopes, H. Madsen, Stochastic nonlinear modelling and application of price-based energy flexibility, Applied Energy 275 (2020) 115096. `doi:https://doi.org/10.1016/j.apenergy.2020.115096`.

[17] J. Mathieu, S. Koch, D. Callaway, State estimation and control of electric loads to manage real-time energy imbalance, in: 2013 IEEE Power Energy Society General Meeting, 2013, pp. 1–1. `doi:10.1109/PESMG.2013.6672144`.

[18] Y. Chen, A. Bušić, S. Meyn, State estimation and mean field control with application to demand dispatch, in: 2015 54th IEEE Conference on Decision and Control (CDC), 2015, pp. 6548–6555. `doi:10.1109/CDC.2015.7403251`.

[19] S. P. Meyn, P. Barooah, A. Bušić, Y. Chen, J. Ehren, Ancillary service to the grid using intelligent deferrable loads, IEEE Transactions on Automatic Control 60 (11) (2015) 2847–2862. `doi:10.1109/TAC.2015.2414772`.

[20] B. Zhang, J. Baillieul, A packetized direct load control mechanism for demand side management, in: 2012 IEEE 51st IEEE Conference on Decision and Control (CDC), 2012, pp. 3658–3665. `doi:10.1109/CDC.2012.6427392`.

[21] B. Zhang, J. Baillieul, A novel packet switching framework with binary information in demand side management, in: 52nd IEEE Conference on Decision and Control, 2013, pp. 4957–4963. `doi:10.1109/CDC.2013.6760667`.

[22] M. Almassalkhi, J. Frolik, P. Hines, Packetized energy management: Asynchronous and anonymous coordination of thermostatically controlled loads, in: 2017 American Control Conference (ACC), 2017, pp. 1431–1437. `doi:10.23919/ACC.2017.7963154`.

[23] M. Almassalkhi, L. D. Espinosa, P. D. H. Hines, J. Frolik, S. Paudyal, M. Amini, Asynchronous Coordination of Distributed Energy Resources with Packetized Energy Management, Springer New York, New York, NY, 2018, pp. 333–361. `doi:10.1007/978-1-4939-7822-9_14`.

[24] L. A. Duffaut Espinosa, M. Almassalkhi, A packetized energy management macro-model with quality of service guarantees for demand-side resources, IEEE Transactions on Power Systems 35 (5) (2020) 3660–3670. `doi:10.1109/TPWRS.2020.2981436`.

[25] H. Mavalizadeh, L. A. Duffaut Espinosa, M. R. Almassalkhi, Decentralized frequency control using packet-based energy coordination, in: 2020 IEEE International Conference on Communications, Control, and Computing Technologies for Smart Grids (SmartGridComm), 2020, pp. 1–7. `doi:10.1109/SmartGridComm47815.2020.9302972`.

[26] J. Frolik, P. Hines, Random access, electric vehicle charge management, in: 2012 IEEE International Electric Vehicle Conference, 2012, pp. 1–4. `doi:10.1109/IEVC.2012.6183162`.

[27] S. P. Mohammad Asif Iqbal Khan, M. Almassalkhi, Performance evaluation of network-admissible demand dispatch in multi-phase distribution grids, in: 2022 IREP Symposium Bulk Power System Dynamics and Control, 2022, pp. 1–8.

[28] M. Almassalkhi, J. Frolik, P. Hines, Packetizing the power grid: The rules of the internet can also balance electricity supply and demand, IEEE Spectrum 59 (2) (2022) 42–47. `doi:10.1109/MSPEC.2022.9706403`.

[29] A. Khurram, M. Amini, L. A. D. Espinosa, P. D. H. Hines, M. R. Almassalkhi, Real-time grid and der co-simulation platform for testing large-scale der coordination schemes, IEEE Transactions on Smart Grid 13 (6) (2022) 4367–4378. `doi:10.1109/TSG.2022.3184491`.

[30] W. Kampel, B. Aas, A. Bruland, Energy-use in norwegian swimming halls, Energy and Buildings 59 (2013) 181–186. `doi:https://doi.org/10.1016/j.enbuild.2012.11.011`.

[31] X. Yuan, L. Lindroos, J. Jokisalo, R. Kosonen, Y. Pan, H. Jin, Demand response potential of district heating in a swimming hall in finland, Energy and Buildings 248 (2021) 111149. `doi:https://doi.org/10.1016/j.enbuild.2021.111149`.

[32] M. Banaei, F. D'Ettorre, R. Ebrahimy, S. A. Pourmousavi, E. M. Blomgren, H. Madsen, A stochastic methodology to exploit maximum flexibility of swimming pool heating systems, International Journal of Electrical Power and Energy Systems 145 (2023) 108643. `doi:https://doi.org/10.1016/j.ijepes.2022.108643`.

[33] L. A. Duffaut Espinosa, M. Almassalkhi, P. Hines, J. Frolik, System properties of packetized energy management for aggregated diverse resources, in: 2018 Power Systems Computation Conference (PSCC), 2018, pp. 1–7. `doi:10.23919/PSCC.2018.8442954`.

[34] N. Zemtsov, J. Hlava, G. Frantsuzova, H. Madsen, R. G. Junker, J. B. Jogensen, Economic mpc based on lpv model for thermostatically controlled loads, in: 2017 International Siberian Conference on Control and Communications (SIBCON), 2017, pp. 1–5. `doi:10.1109/SIBCON.2017.7998560`.

[35] M. Banaei, R. Ebrahimy, H. Madsen, Two-stage secure bottom-up load coordination mechanism in distribution grids, in: 2023 IEEE 11th International Conference on Smart Energy Grid Engineering (SEGE), 2023, pp. 64–69. `doi:10.1109/SEGE59172.2023.10274586`.

[36] Nord pool day-ahead market prices, `https://www.nordpoolgroup.com/en/Market-data1/Dayahead/Area-Prices/ALL1/Hourly1/?view=table`, accessed: 2022-09-27 (2022).

[37] J. Yasuoka, J. A. Jardini, J. L. P. Brittes, L. C. Magrini, P. S. D. Kayano, J. de Camargo, Assessment of the allowable short-term overloads in power transformers including condition management, in: CIRED 2005 - 18th International Conference and Exhibition on Electricity Distribution, 2005, pp. 1–4. `doi:10.1049/cp:20051106`.